

LETTER

Simultaneous determination of effective carrier lifetime and resistivity of Si wafers using the nonlinear nature of photocarrier radiometric signals

To cite this article: Qiming Sun *et al* 2018 *J. Phys. D: Appl. Phys.* **51** 15LT01

View the [article online](#) for updates and enhancements.

Related content

- [Investigation of recombination parameters in silicon structures by infrared and microwave transient absorption techniques](#)
E Gaubas, A Kaniava and J Vaitkus
- [Photocarrier radiometry for noncontact evaluation of space monocrystalline silicon solar cell under low-energy electron irradiation](#)
Liu Jun-Yan, Peng Song, Wang Fei *et al.*
- [Nonlinear photothermal modulated optical reflectance and photocurrent phenomena in crystalline semiconductors: I. Theoretical](#)
Robert E Wagner and Andreas Mandelis

Recent citations

- [Contactless non-destructive imaging of doping density and electrical resistivity of semiconductor Si wafers using lock-in carrierography](#)
Peng Song *et al*



IOP | ebooks™

Bringing together innovative digital publishing with leading authors from the global scientific community.

Start exploring the collection—download the first chapter of every title for free.

Letter

Simultaneous determination of effective carrier lifetime and resistivity of Si wafers using the nonlinear nature of photocarrier radiometric signals

Qiming Sun^{1,2} , Alexander Melnikov², Jing Wang¹ and Andreas Mandelis^{1,2,3}

¹ School of Optoelectronic Science and Engineering, University of Electronic Science and Technology of China, Chengdu 610054, People's Republic of China

² Center for Advanced Diffusion-Wave and Photoacoustic Technologies (CADIPT), University of Toronto, Toronto, ON M5S 3G8, Canada

E-mail: mandelis@mie.utoronto.ca

Received 24 December 2017, revised 28 February 2018

Accepted for publication 2 March 2018

Published 19 March 2018



CrossMark

Abstract

A rigorous treatment of the nonlinear behavior of photocarrier radiometric (PCR) signals is presented theoretically and experimentally for the quantitative characterization of semiconductor photocarrier recombination and transport properties. A frequency-domain model based on the carrier rate equation and the classical carrier radiative recombination theory was developed. The derived concise expression reveals different functionalities of the PCR amplitude and phase channels: the phase bears direct quantitative correlation with the carrier effective lifetime, while the amplitude versus the estimated photocarrier density dependence can be used to extract the equilibrium majority carrier density and thus, resistivity. An experimental 'ripple' optical excitation mode (small modulation depth compared to the dc level) was introduced to bypass the complicated 'modulated lifetime' problem so as to simplify theoretical interpretation and guarantee measurement self-consistency and reliability. Two Si wafers with known resistivity values were tested to validate the method.

Keywords: photocarrier radiometry, nonlinearity, carrier lifetime, resistivity

(Some figures may appear in colour only in the online journal)

1. Introduction

The electronics industry has become one of the largest in the world and characterization techniques for materials and devices are proportionally in great demand, aimed at providing performance assessment and quality control at all stages of research, fabrication, and manufacturing [1, 2]. As an important category of semiconductor properties, carrier transport

and recombination parameters such as lifetimes and diffusion lengths are being routinely measured in modern micro-, nano- and opto-electronics industry. Owing to the importance of characterization methods, a deeper physical insight into carrier dynamics and kinetics involved in the various parameter measurements for rigorous interpretation of their results are of great interest with a goal to improve measurement self-consistency and reliability [2–5].

Most all-optical dynamic characterization techniques feature nondestructive, noncontact, fast, and stand-alone

³ Author to whom any correspondence should be addressed.

quantitative capability (calibration free), and are thus very promising for industrial in-line inspection. One of the key physics challenges with optical characterization techniques is the nonlinear response of detected signals with respect to excitation/carrier injection, which is physically inherent and has been generally observed [3, 6–10]. Although it has been customary to just quote a single numerical value for a certain semiconductor parameter, rigorously speaking almost all photocarrier transport and recombination parameters, including the surface recombination velocity, the bulk lifetime, the carrier diffusivity, and the effective lifetime, are not constant and are functions of the photocarrier injection level. Under these circumstances, for dynamic techniques where the excitation is pulsed/modulated, the carrier recombination parameters will also vary with the excitation waveform even at low injection levels, leading to complicated nonlinear problems for both experimental condition control and theoretical interpretation. Plenty of efforts have been made during the past few decades to deal with this issue [11–15].

Photocarrier radiometry (PCR) [16] and its imaging counterpart lock-in carrierography [17], a frequency-domain (FD) photoluminescence (PL) based quantitative characterization technique that measures photocarrier density distributions, has been demonstrated to be capable of characterizing carrier recombination properties [18–20], mobility/diffusivity [21, 22], ion implantation dose [23], junction properties [24, 25], and trap states/activation energy [26, 27] in various semiconductor materials and devices. However, PCR shares the same nonlinearity issues as other dynamic optical techniques, which may substantially compromise its theoretical rigor and measurement self-consistency and reliability.

This report is dedicated to the study and measurement-related benefits of the nonlinear behavior of PCR signals in c-Si characterization, in which the origins of the nonlinearity can be basically attributed to: (1) a nonlinear correlation between the excitation intensity and the photocarrier density that can be effectively described as an injection-level-dependent carrier effective lifetime [5, 13, 14]; and (2) a nonlinear correlation between the photocarrier density and the PL intensity [28, 29]. If the former is dealt with correctly, the measurement benefit will be the self-consistent estimate of the carrier effective lifetime and the absolute injected photocarrier density. If the latter is correctly identified, it will lead to the measurement of electrical resistivity in an all-optical non-contacting manner.

Compared to other PL-based techniques aiming at measuring effective lifetime and/or majority carrier density/resistivity [13, 15, 29–31], the method presented in this work features a clearer physical picture and more simplified theoretical/computational treatment without loss of rigor: a ‘ripple’ mode excitation was introduced that helps bypass the complicated parameter nonlinearity problem caused by the non-constant effective lifetime, thereby enabling a highly simplified computation and data interpretation. The use of a FD PCR model developed herein provides a closed-form concise solution based on Fourier transformation and the convolution theorem and reveals direct quantitative correlations among PCR

amplitude, PCR phase, effective lifetime, and equilibrium majority carrier density. Finally, lock-in amplifier-mediated PCR signal demodulation provides FD information that features superior SNR to software-based time-domain (TD) curvature analysis techniques.

2. Theory

PL intensity from doped semiconductors is proportional to the product of the minority and the majority carrier density [28]

$$S(t) = C[\Delta n(t) + n_0][\Delta p(t) + p_0] \approx C\Delta n(t)[\Delta n(t) + N_d] \quad (1)$$

where C is a proportionality factor, $\Delta n(t)$ and $\Delta p(t)$ the photogenerated excess electron and hole densities, respectively, n_0 and p_0 the equilibrium electron and hole densities, respectively, and N_d the equilibrium majority carrier (either electron or hole) density due to doping. The factor C takes all the proportionality factors into account such as the band-to-band carrier radiative recombination coefficient, the surface reflectivity of samples with respect to the near-infrared PL, the PL detection solid angle, the responsivity of the PL detector etc. The latter part of equation (1) is based on two assumptions/approximations: (1) the photogenerated excess minority carrier density is much higher than the equilibrium minority carrier density; and (2) the excess minority carrier density and the excess majority carrier density are equal (quasi-neutrality state). These two approximations are valid for most cases in PCR characterization of Si wafers. Consequently, $\Delta n(t)$ can be generally identified with the carrier density wave (CDW) [16, 32], not specifically referring to the electron or hole density.

In our experiments, the wavelength of the laser excitation was 808 nm, corresponding to an optical absorption depth on the order of 10 μm in crystalline Si. This absorption depth is much shorter than both the wafer thickness and the carrier diffusion length; as a result, the optical absorption can be considered as a surface absorption. For the case of sine-wave-modulated and homogenized (1D) laser excitation, the depth-averaged carrier generation rate can be expressed as

$$G(t) = \frac{I_0(1-R)}{E_0L}(1 + \gamma \cos \omega t) \equiv \sum_{k=-1}^1 G_k e^{ik\omega t}, \quad 0 < \gamma \leq 1 \quad (2)$$

where I_0 is the average laser intensity, R the reflectivity (0.32 for 808 nm light incident on polished Si wafer surfaces [33]), E_0 the photon energy, L the wafer thickness, γ the amplitude modulation depth factor, ω the angular modulation frequency, and G_k the Fourier coefficient of the carrier generation rate, subject to the relation $G_1 = G_{-1} = \gamma G_0/2 = \gamma I_0(1-R)/(2E_0L)$. Here, γ is introduced to describe the ripple mode used in our experiments (small optical modulation depth compared to the dc level). Equation (2) holds for the case where L is smaller than or compared to the carrier diffusion length L_D (the case in this study); for the case $L \gg L_D$ (e.g. Si ingot), it is more reasonable to replace L by L_D in equation (2).

The relation between $\Delta n(t)$ and $G(t)$ is governed by the carrier rate equation

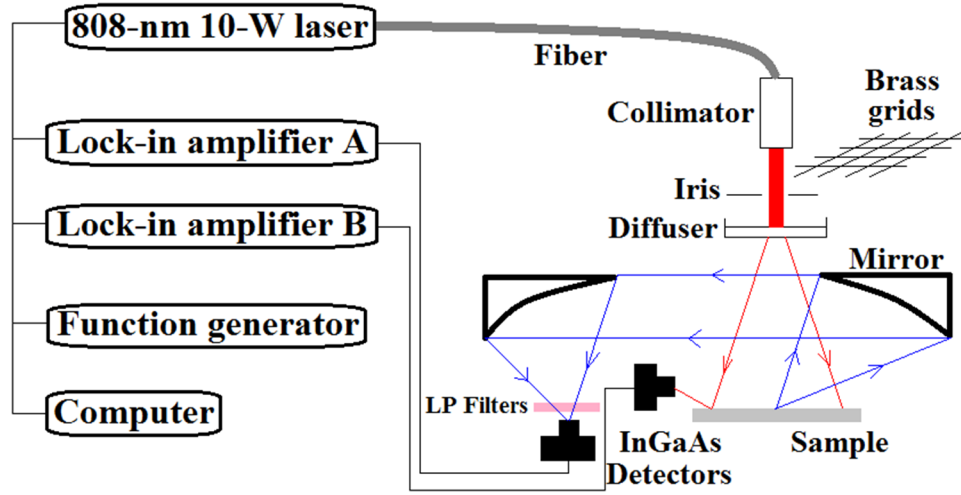


Figure 1. Schematic of the experimental intensity-scanned PCR system.

$$\frac{d\Delta n(t)}{dt} = G(t) - \frac{\Delta n(t)}{\tau_e(\Delta n(t))} \quad (3)$$

where τ_e is the effective lifetime which lumps all the carrier recombination rates together such as Shockley–Read–Hall (SRH) bulk recombination, SRH surface recombination, electron–hole radiative recombination, Auger recombination etc. Although the fact that $\tau_e = \tau_e(\Delta n(t))$ renders a general closed-form solution of equation (3) impossible [3, 13], under the ripple mode where γ is very small and accordingly G_1 is much smaller than G_0 , this lifetime dependence is approximately reduced to $\tau_e \approx \tau_e(\Delta n_0)$, where Δn_0 is the dc component (not modulated) of the CDW. Then the FD solution of equation (3) can be expressed as

$$\Delta n(t) \approx \sum_{k=-1}^1 \Delta n_k e^{ik\omega t}, \quad \text{where } \Delta n_k = \frac{G_k \tau_e(\Delta n_0)}{1 + ik\omega \tau_e(\Delta n_0)}. \quad (4)$$

Here, higher harmonics of the CDW were assumed to be negligible compared to the dc and the first harmonic components by virtue of the ripple mode. It is noted that Δn_{-1} is the complex conjugate of Δn_1 .

The PCR signal (the fundamental-frequency component of the detected PL, extracted by the lock-in amplifier) can be derived by Fourier transforming equation (1), with the rhs of equation (1) being in the form of FD convolution due to the multiplication in TD

$$\begin{aligned} S(\omega) &= \int_{-\infty}^{\infty} C \Delta n(\omega') [\Delta n(\omega - \omega') + N_d \delta(\omega - \omega')] d\omega' \\ &= C(2\Delta n_0 + N_d) \Delta n_1 \end{aligned} \quad (5)$$

where δ is the Dirac function. By simple manipulations, the amplitude A and the phase φ of the PCR signal can be separated out from equation (5)

$$\begin{cases} A = \frac{C\gamma(2\Delta n_0 + N_d)\Delta n_0}{2\sqrt{1 + \omega^2 \tau_e^2}} \\ \tan \varphi = -\omega \tau_e \end{cases}. \quad (6)$$

From equation (6), one can see that the effective lifetime can be directly calculated from the phase, with known

modulation frequency $f = \omega/2\pi$. In addition, we also obtain the relation that the amplitude A multiplying the coefficient $(1 + \omega^2 \tau_e^2)^{-1/2}$ (referred to as the normalized amplitude in what follows) is proportional to $(2\Delta n_0 + N_d)\Delta n_0$, indicating that a plot of the amplitude versus Δn_0 ($\Delta n_0 = G_0 \tau_e$) can be used to extract N_d . The quantitative correlation between Si wafer resistivity and N_d has been well established for various dopants [2].

It is worth noting that all the parameters introduced above are depth averaged, independent of the depth coordinate. Although the solution of the more rigorous carrier diffusion-wave partial differential equation combined with the two surface recombination boundary conditions has been fully derived for the ideal case where all the carrier recombination and transport parameters are constant [32], in view of the fact that in practice these carrier parameters are generally injection level dependent, one has to use the depth averaged equation and parameters such as the effective lifetime in order to obtain closed-form expressions.

Based on the above analysis, the route to determining lifetime and resistivity using PCR now becomes apparent: (1) run a ripple-mode intensity scan at a selected frequency satisfying the quasi-steady-state condition [3]; (2) calculate the τ_e versus I_0 dependence from the phase data using equation (6); (3) with known G_0 and τ_e , estimate Δn_0 through equation (4); and (4) plot the amplitude versus Δn_0 data curve and use equation (6) for best fitting to extract the N_d value. The lifetime measured here is clearly defined as the actual value corresponding to the level of the dc component of the modulated photocarrier density.

3. Experimental

A schematic of the PCR experimental system is shown in figure 1. An 808 nm laser with 10 W average power was modulated and used as the optical excitation source, with the modulation amplitude factor $\gamma = 1$ for the regular mode and $\gamma = 0.1$ for the ripple mode. The laser beam was spread and homogenized by a diffuser to shape a $5 \times 5 \text{ cm}^2$ spot on wafer

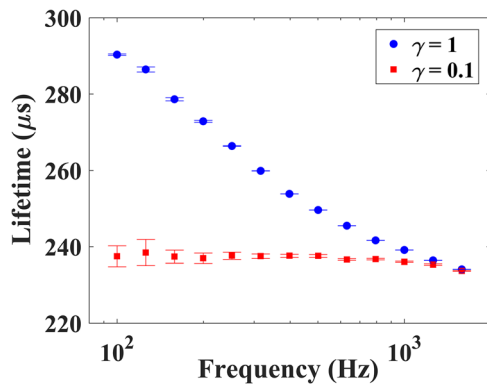


Figure 2. Comparison of lifetime measurements between the regular ($\gamma = 1$) and the ripple ($\gamma = 0.1$) modes.

samples. The excitation intensity was changed through adding brass grids (50% transmittance for each) and continuously adjusting the iris (the laser intensity distribution on the sample surface was not changed by virtue of the diffuser). The sample temperature rise under these illumination levels was roughly estimated to be less than 50 °C, so the influence of heating on the sample electronic properties is negligible.

An InGaAs detector was used to monitor the relative intensity change by measuring the reflected beam, while another InGaAs detector was used to measure PCR signals with two 1000 nm long-pass filters placed in front of it in order to block the excitation beam. The InGaAs detector has a spectral range of 900–1700 nm, so the wavelength range for the PL signal detection was approx. from 1000 to 1700 nm. Two lock-in amplifiers demodulated the detector output signals and provided amplitude and phase information. The time constant of both lock-in amplifiers was set at 3 s.

Two c-Si wafers were tested: Sample No. 1 was n-type, 290 μm -thick, with both surfaces partly passivated with a 30 nm amorphous-Si layer, and $1 \Omega \cdot \text{cm}$ nominal resistivity provided by the manufacturer; Sample No. 2 was p-type, 690 μm -thick, with both surfaces passivated with thick oxides, and 20–40 $\Omega \cdot \text{cm}$ nominal resistivity also provided by the manufacturer.

4. Results and discussion

A comparison of the effective lifetime measurements as a function of frequency between the regular ($\gamma = 1$) and the ripple ($\gamma = 0.1$) modes shown in figure 2 corroborates the importance and the effectiveness of the ripple mode in terms of the ‘modulated lifetime’ issue. The lifetime values in figure 2 were calculated from the PCR phase data using equation (6). The ripple-mode lifetime is almost constant from 100 Hz to 1 kHz, while the regular-mode lifetime decreases versus frequency and gradually converges to the ripple-mode value, due to the damping of the CDW amplitude at high frequencies [32]. Above 1 kHz, the ripple mode lifetime (and also the regular mode lifetime) will not be constant, as the quasi-steady-state condition ($\omega\tau_e \ll 1$) will be violated. Therefore, the PCR effective lifetime at low frequencies should be perceived as the quasi-steady-state lifetime [3].

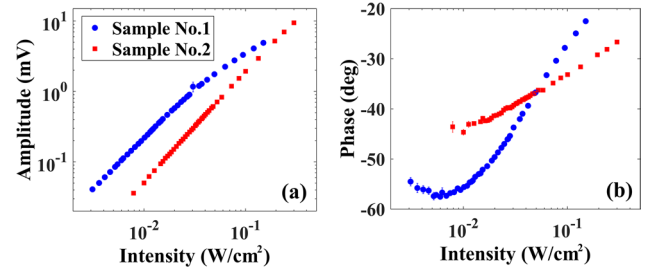


Figure 3. PCR intensity-scan data of the two wafer samples: (a) amplitude versus intensity dependence; (b) phase versus intensity dependence. The intensity values on the x -axis are the average intensities (dc level) of the sine-wave modulated laser excitation. The modulation frequency was 100 Hz for Sample No. 1, and 200 Hz for Sample No. 2.

PCR intensity-scan amplitude and phase data of the two samples are shown in figure 3. The modulation frequency was chosen to be 100 Hz for Sample No. 1 and 200 Hz for Sample No. 2. The reasons for selecting these frequencies are: (1) for frequencies much lower than those, the corresponding PCR phases are close to zero [32], leading to limited dynamic range of phase data; and (2) the noise spectrum of the PCR experimental system is usually Gaussian, so the noise level at lower frequencies will be greater. From figure 3(b), one can see that the phases of the two samples are very sensitively intensity dependent, indicating the existence of a strong nonlinearity caused by the injection-level-dependent effective carrier lifetime.

According to equation (6), each phase datum corresponds to a carrier effective lifetime, so the phase data in figure 3(b) can be directly converted to lifetime dependence on intensity as shown in figure 4. The effective lifetime of Sample No. 1 was generally longer than that of Sample No. 2, due to the higher effectiveness of amorphous-Si surface passivation than oxidation passivation [24]. The negative correlations of lifetime versus intensity observed in figure 4 are due to Auger recombination dominating the various carrier recombination processes at high injection levels. The positive correlation segment of the Sample No. 1 lifetime at low intensities can be attributed to dominant SRH recombination processes at relatively low injection levels [3]. Further analysis of the determination of parameters such as the Auger coefficient and the density of SRH recombination centers was developed but is outside the scope of this report.

The absolute injected photocarrier density shown on the x -axis of figure 4 was scaled from the excitation intensity information shown in figure 3, using the calculated effective carrier lifetime combined with equation (4). Here, the photocarrier density is the dc level of the modulated CDW. With knowledge of the absolute photocarrier density, and combined with the yet unused PCR intensity-scan amplitude data shown in figure 3(a), the normalized amplitude versus photocarrier dependence can be plotted as the data set required for the determination of the equilibrium majority carrier density / resistivity. The results are shown in figure 5. One can see that the dependencies in figure 5 have the form of

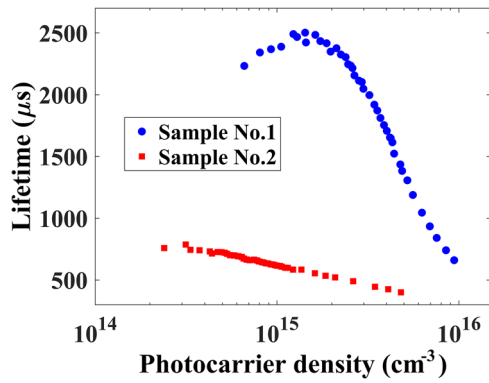


Figure 4. Effective lifetime as a function of dc photocarrier density calculated from the intensity-scan phase data using equations (4) and (6).

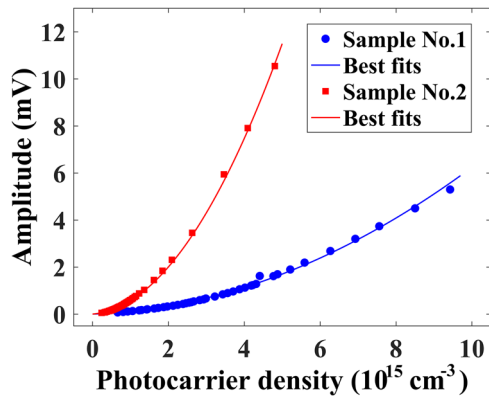


Figure 5. Normalized amplitude versus photocarrier density data and the corresponding theoretical best-fitted curves using equation (6). Normalized amplitude means the amplitude measured by the lock-in amplifier multiplies the coefficient $(1 + \omega^2 \tau_c^2)^{-1/2}$, as seen in equation (6). The fitted N_d value was $2.0 \times 10^{15} \text{ cm}^{-3}$ for Sample No. 1, and $6.4 \times 10^{14} \text{ cm}^{-3}$ for Sample No. 2.

a second-order polynomial, as expected from equation (6). By best fitting equation (6) to the data, it was found that the equilibrium majority carrier densities of Sample Nos. 1 and 2 were $(2.0 \pm 0.2) \times 10^{15}$ and $(6.4 \pm 0.3) \times 10^{14} \text{ cm}^{-3}$, respectively. Using the empirical formulas given in [2], the resistivity values of the two samples were found to be (2.3 ± 0.2) and $(20.8 \pm 0.8) \Omega \cdot \text{cm}$, respectively, generally consistent with the nominal resistivity values provided by the wafer manufacturers.

The intensity-scan range for resistivity determination should be at the intermediate carrier injection level, i.e. the injected photocarrier density Δn_0 should be on the order of the equilibrium majority carrier density N_d , where the amplitude versus photocarrier density plot is most sensitive to N_d . Otherwise, if $\Delta n_0 \ll N_d$, then, according to equation (6), the data dependence will be almost linear, and one cannot separate N_d from the slope of the linear dependence which also depends on the proportionality factor C ; if $\Delta n_0 \gg N_d$, then the data will be almost independent of N_d , as the equilibrium majority carriers are overwhelmed by the minority photocarriers raised by the laser, and subsequently a small experimental data error may cause a significant deviation of N_d from its actual value.

A four-point-probe resistivity measurement on the unpassivated part of Sample No. 1 was performed in order to compare with the PCR results. The resistivity value was found to be $1.54 \Omega \cdot \text{cm}$. The difference of the results between the two techniques may be partly due to the different measurement locations on Sample No. 1 as wafer resistivity may have a non-uniform distribution: the area where the resistivity was measured by PCR is not accessible to the four-point-probe method, as the surface passivation layer acts as an insulating layer; conversely, the area measured by the four-point-probe method (bare Si surface) is difficult for PCR probing, as the PCR signals from surface-unpassivated areas exhibited more complicated behaviors such as unstable amplitudes and phases due to interactions between semiconductor surface and laser irradiation [34]. Sample No. 2 was totally inaccessible to the four-point-probe method because the entire wafer surface was oxidation passivated.

The influence of the surface passivation layers on the photocarrier generation is negligible due to the fact that both the optical absorption length and the carrier diffusion length are much longer than the surface layer thickness; on the other hand, the effect of the surface layer on carrier recombination can be approximately treated as a surface recombination velocity or an effective carrier lifetime, the latter being measured in this work. The influence of the surface layers on the PCR measured resistivity values is also negligible, as most of the photocarrier generation, diffusion, and recombination occur in the wafer bulk. This fact allows another bulk property, the equilibrium majority carrier density (directly correlated to the resistivity), to be extracted.

5. Conclusions

A theoretically and experimentally rigorous treatment of the nonlinear behavior of PCR signals was developed, and the specific experimental and computational steps/conditions necessary for assuring the validity of the measurements were identified. The effectiveness of the experimental ripple-mode excitation and the corresponding theoretical treatment proposed in this paper is not restricted to PCR characterization of Si materials and devices but is also generally applicable to other modulated diagnostic techniques and other semiconductor materials involving either the nonlinear correlation between generation rate and excess carrier density or the nonlinear correlation between excess carrier density and measured signals. The developed methodology for wafer resistivity measurements can be used as a complement to conventional contacting electrical methods, but also as a stand-alone method in cases where electrical measurements cannot be obtained, such as with oxidized or surface treated wafers.

Acknowledgments

The authors are grateful to the Natural Sciences and Engineering Research Council of Canada (NSERC) for a Discovery grant, to the Canada Foundation for Innovation

(CFI) for equipment grants, to the Canada Research Chairs Program, and to the Chinese Recruitment Program of Global Experts (Thousand Talents). QMS and JW acknowledge the NSFC (Grant Nos. 61601092, 61771103, and 61704023).

ORCID iDs

Qiming Sun  <https://orcid.org/0000-0003-1184-3719>

References

- [1] Sze S M and Ng K K 2007 *Physics of Semiconductor Devices* (New York: Wiley)
- [2] Schroder D K 2006 *Semiconductor Material and Device Characterization* (New York: Wiley)
- [3] Giesecke J 2014 *Quantitative Recombination and Transport Properties in Silicon From Dynamic Luminescence* (Heidelberg: Springer)
- [4] Kirchartz T, Helbig A and Rau U 2008 *Sol. Energy Mater. Sol. Cells* **92** 1621
- [5] Sinton R A and Trupke T 2012 *Prog. Photovolt., Res. Appl.* **20** 246
- [6] Brendel R 1995 *Appl. Phys. A* **60** 523
- [7] Macdonald D and Cuevas A 1999 *Appl. Phys. Lett.* **74** 1710
- [8] Tolev J, Mandelis A and Pawlak M 2007 *J. Electrochem. Soc.* **154** H983
- [9] Sun Q M, Melnikov A and Mandelis A 2016 *Phys. Status Solidi a* **213** 405
- [10] Hu L L, Yang Z Y, Mandelis A, Melnikov A, Lan X Z, Walters G, Hoogland S and Sargent E H 2016 *J. Phys. Chem. C* **120** 14416
- [11] Schmidt J 1999 *IEEE Trans. Electron Devices* **46** 2018
- [12] Trupke T and Bardos R A 2004 *Appl. Phys. Lett.* **85** 3611
- [13] Trupke T, Bardos R A and Abbott M D 2005 *Appl. Phys. Lett.* **87** 184102
- [14] Giesecke J A, Niewelt T, Rudiger M, Rauer M, Schubert M C and Warta W 2012 *Sol. Energy Mater. Sol. Cells* **102** 220
- [15] Giesecke J A, Schubert M C and Warta W 2012 *Phys. Status Solidi a* **209** 2286
- [16] Mandelis A, Batista J and Shaughnessy D 2003 *Phys. Rev. B* **67** 205208
- [17] Sun Q M, Melnikov A and Mandelis A 2012 *Appl. Phys. Lett.* **101** 242107
- [18] Wang J, Mandelis A, Melnikov A, Hoogland S and Sargent E H 2013 *J. Phys. Chem. C* **117** 23333
- [19] Sun Q M, Melnikov A, Mandelis A and Pagliaro R H 2018 *Appl. Phys. Lett.* **112** 012105
- [20] Hu L L, Liu M X, Mandelis A, Sun Q M, Melnikov A and Sargent E H 2018 *Sol. Energy Mater. Sol. Cells* **174** 405
- [21] Batista J, Mandelis A and Shaughnessy D 2003 *Appl. Phys. Lett.* **82** 4077
- [22] Hu L L, Liu M X, Mandelis A, Melnikov A and Sargent E H 2017 *Prog. Photovolt., Res. Appl.* **25** 1034
- [23] Shaughnessy D, Li B C, Mandelis A and Batista J 2004 *Appl. Phys. Lett.* **84** 5219
- [24] Melnikov A, Halliop B, Mandelis A and Kherani N P 2012 *Thin Solid Films* **520** 5309
- [25] Melnikov A, Mandelis A, Halliop B and Kherani N P 2013 *J. Appl. Phys.* **114** 244506
- [26] Wang J, Mandelis A, Melnikov A and Sun Q M 2016 *Int. J. Thermophys.* **37** 60
- [27] Hu L L, Mandelis A, Yang Z Y, Guo X X, Lan X Z, Liu M X, Walters G, Melnikov A and Sargent E H 2017 *Sol. Energy Mater. Sol. Cells* **164** 135
- [28] Roosbroeck W V and Shockley W 1954 *Phys. Rev.* **94** 1558
- [29] Giesecke J A, Schubert M C and Warta W 2012 *J. Appl. Phys.* **112** 063704
- [30] Mitchell B, Trupke T, Weber J W and Nyhus J 2011 *J. Appl. Phys.* **109** 083111
- [31] Hameiri Z, Trupke T, Gao N, Sinton R A and Weber J W 2013 *Prog. Photovolt., Res. Appl.* **21** 942
- [32] Mandelis A 2001 *Diffusion-Wave Fields* (New York: Springer)
- [33] Green M A and Keevers M J 1995 *Prog. Photovolt., Res. Appl.* **3** 189
- [34] Wang Q and Li B C 2016 *Int. J. Thermophys.* **37** 39